Open material database for tensile test properties of additive manufacturing materials

A A Garcia-Granada[1,*], H. Rostro-González[1], J M Puigoriol-Forcada[1] and G Reyes-Pozo[1]

[1] Grup d'Enginyeria en Producte Industrial (GEPI), Institut Químic de Sarrià, Universitat Ramon Llull, Via Augusta 390, 08017 Barcelona, Spain

[*]andres.garcia@iqs.url.edu

Abstract. In recent years, the investigation of material properties within additive manufacturing, also known as 3D printing, has gained significant research attention. The intricate interplay between numerous fabrication parameters and the resultant material properties of 3D-printed components has become crucial, particularly for enabling effective topology optimization. Considering this, we propose the establishment of an accessible open database. This repository stores a comprehensive collection of fabrication files corresponding to each distinct material and printer combination, accompanied by the outcomes of meticulous tensile testing. To support the research community, our initiative extends to the inclusion of material provider datasheets, facilitating comprehensive result comparisons. A standardized approach utilizing consistently applied strain rates is recommended, focusing on a compact dog bone specimen design. This pioneering attempt encompasses an expansive array of data derived from 25 distinct materials and 9 diverse printers, meticulously capturing the inherent variability within the samples. The database catalogues the complete spectrum of tensile test data, encompassing various essential measurements such as mass, and crucial material properties including Young's modulus, yield stress, fracture strain, and absorbed energy. These recorded metrics can be seamlessly correlated against density, manufacturing time, or cost parameters, enabling the generation of insightful plots and analysis. Through this collaborative effort, we aim to provide researchers with a robust foundation for informed decision-making and advancements in additive manufacturing.

1. Introduction

Additive manufacturing has emerged as a revolutionary technique, allowing the production of individual components without the reliance on traditional tooling methods such as molds for plastic injection or matrices for metal stamping [1,2]. For these materials you can find many sorts of database such as https://www.matweb.com/, https://www.campusplastics.com/ and material selection software such as https://www.grantadesign.com/. Additive manufacturing is experiencing a rapid expansion in various applications, driven by the advent of novel printers, transformative technologies, and an evolving spectrum of materials [3,4]. Nevertheless, the successful utilization of additive manufacturing demands a comprehensive understanding of material properties, which exhibit notable variations contingent upon

distinct manufacturing parameters [5]. For example, in the pursuit of optimal material properties for additive manufacturing, Garcia-Granada et al. [6] encountered challenges in implementing topology optimization. Their comparative study of two high-performance 3D printing machines revealed intriguing insights. The success of optimization was evident in the case of a Fortus 400mc employing Fused Deposition Modeling (FDM) technology, utilizing ABS-M30 material. However, the same level of optimization eluded the Polyjet Objet30 Prime printer, even with the utilization of Verowhite material. FDM is a trademarked term owned by Stratasys, a 3D printing company. Fused Filament Fabrication (FFF) is a generic term that describes the same technology.

In the realm of advanced manufacturing, FDM stands as a pioneering technique that holds immense promise for the fabrication of thermoplastic polymer composites. The synergy of thermoplastic polymers with composite materials presents a compelling avenue for achieving enhanced mechanical, thermal, and functional properties [7]. Domingo-Espin et al. [8] have made significant progression in unraveling the complexities of fused deposition modeling for polycarbonate parts. Through meticulous experimentation, they have discerned that the Young's modulus can fluctuate within a range of ±10%, a phenomenon attributed to the orientation during printing. Similarly, tensile strength exhibited variations of up to ±20%, while ultimate strain displayed a significant scatter, spanning from as low as 2% to a substantial 11.8%. On the tensile testing, a review of additively manufactured polymers is given in [9]. In this paper, it becomes evident that a significant gap exists in the realm of suitable standards designed to systematically evaluate the tensile properties of polymer components. This gap is particularly conspicuous when considering the intricate landscape of Fused Filament Fabrication (FFF), where the mechanical behavior is intricately governed by a multitude of printing parameters [10]. The inadequacy of existing standards becomes apparent in their inability to encompass the diverse array of influential factors that contribute to the mechanical characteristics of FFF-produced parts [11].

There is a need to document all sort of material properties for additive manufacturing such as thermal conductivity [12], viscoelastic properties [13], conductive properties [14].

The substantial diversity in printing parameters, printer models, and material properties is the focal point of our efforts in this work. To address this multifaceted challenge, we propose the creation of a comprehensive database that incorporates many of the key factors discussed here. This database is poised to serve as a foundational resource in the field of additive manufacturing.

Our initial iteration of this additive manufacturing database, denoted as Version 01, is now accessible via the following link: https://meaagg.com/AMDB/AMDB.html. This repository stands as an invaluable asset, catering to the needs of both researchers and practitioners alike. It streamlines the exploration and integration of critical insights and data within the realm of additive manufacturing, offering a robust platform for advancing knowledge and innovation in this dynamic field.

2. Materials and methods

2.1. Geometry

Tensile tests are performed using a small geometry to minimise the use of material and manufacturing time. The geometric configuration is inspired by the ASTM_D638_V standard, with dimensions set at a thickness of 2 mm and width of 3.18 mm, culminating in a cross-sectional area of 6.36 mm². For precise specifications of an individual tensile specimen, refer to Figure 1a, which requires a material volume of 930 mm³. Length for strain calculation was calibrated using finite element analysis as shown in figure 1c. For a displacement of U=1 mm and E=2000 MPa an average stress of σ=80 MPa was observed in the cross section area. Therefore, for deformation calculations ($\varepsilon=U/L$) we used the length $L=E*U/\sigma$=2000*1/80=25mm.

To streamline the process, an STL file encompassing four specimens has been curated and incorporated into the material database. This strategic optimization minimizes the required printing volume to 5541.19 mm³ (32.03 x 86.50 x 2), while material consumption remains confined to 3720 mm³

(4 x 930). The intricate details of the STL geometry earmarked for printing are meticulously outlined in Figure 1b, with slim 1.14 mm separations thoughtfully incorporated between specimens.

While the adoption of such diminutive specimens offers noteworthy advantages in terms of economizing both time and material resources, it is pertinent to acknowledge a limitation. Regrettably, due to their small size, the ability to investigate the implications of infill patterns is curtailed. This restriction is attributed to the preponderance of slicing utilized for generating outer surfaces, thereby warranting a judicious consideration of the experimental scope and its corresponding constraints.

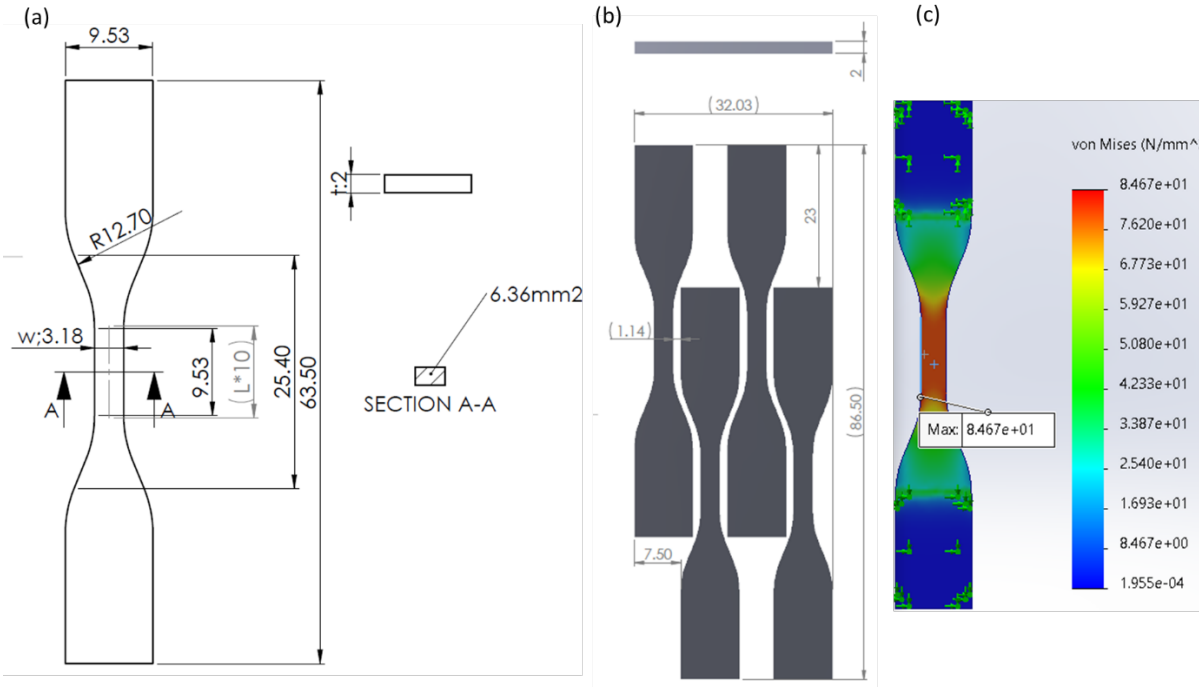

Figure 1. Geometry of (a) 1 tensile specimen and (b) downloaded STL for 4 tensile specimens and (c) length calibration.

2.2. 3D printers and slicing

The material database encompasses a diverse array of printers and slicing methods, accommodating a wide spectrum of choices. A primary premise of this database is to meticulously chronicle crucial details, including the specific material, printer model, slicing technique employed, and the associated manufacturing file. This comprehensive documentation is instrumental in fostering repeatability and ensuring the veracity of the results obtained.

In alignment with the scope of this paper, a specific subset of machines, slicing software, and materials has been judiciously considered, as outlined in Table 1. Each material, within the database, warrants a meticulous record encompassing the printer model utilized, the slicer employed, a visual representation of the slicing process, the manufacturing file itself, and, upon completion of testing, a minimum of four illustrative result images. The column run in material database makes reference to the specimen test run recorded in the tensile test machine.

By adhering to this meticulous documentation framework, the material database not only amplifies the value of this research but also lays a robust foundation for future investigations, augmenting the transparency, reliability, and transferability of findings across diverse additive manufacturing scenarios.

Table 1. 3D printing machine, slicing and material

Technology	Slicing software	Machine	Materials	Run	€/min	€/gr
FFF / FDM	Cura 4.8.0	Ultimaker S5	PLA	135-138	0.02	0.1
			ABS	149-152	0.02	0.1
			TPU	145-148	0.02	0.1
			TPU+ABS	141-144	0.02	0.1
			PCL	186-189	0.02	0.1
		Prusa i3 mk3	PLA	115-119+121-126	0.01	0.1
			ABS	153-156	0.01	0.1
			PETG	191-194	0.01	0.1
			PLAFe	227-232	0.01	0.1
			PETG+PLA	196-199	0.01	0.1
		Ender 3v2	PHA210	238-240	0.01	0.1
			PHA190	234-237	0.01	0.1
	Axon 2	BFB 3000	PLA	131-134	0.01	0.1
			ABS	131b-134b	0.01	0.1
			PP0.5	204-207	0.01	0.1
			PP0.25	200-203	0.01	0.1
	Insight 14.4	Fortus 400mc	ABS-M30	x-x	0.30	1.0
	Cloudprint	Makerbot Method X	Nyloncarbon	176-179	0.10	0.25
SLA	Formlabs 3BL	Preform 3.25	FLEX80A	164-167+217-220	0.10	1.0
			BIO	180-183	0.10	1.0
			ELASTIC50A	168-172	0.10	1.0
			GREY	221-225	0.10	1.0
SLS	Sintratek Kit	Sintratec C1.2	TPU	233	0.02	0.1
Polyjet	Objet 30 Prime	Objet 9.2.8	Verowhite	127-130	0.10	0.25
			Med610	157-160	0.10	0.25
			Tangogrey	161-162+174-175	0.10	0.25

To exemplify the thorough documentation provided within the database, we present two snapshots showcasing the slicing process. Figure 2 captures a snapshot of Cura for Prusa, while Figure 3 displays a snapshot of Preform for Formlabs. These visual representations serve as illustrative instances, showing the intricate slicing strategies employed. The underlying intent is to facilitate direct comparisons, especially when different slicing software solutions are employed. By archiving these insights, the database delights a systematic approach to deciphering the impact of varying slicing methodologies, thus fostering a deeper understanding of the interplay between software choices and additive manufacturing outcomes.

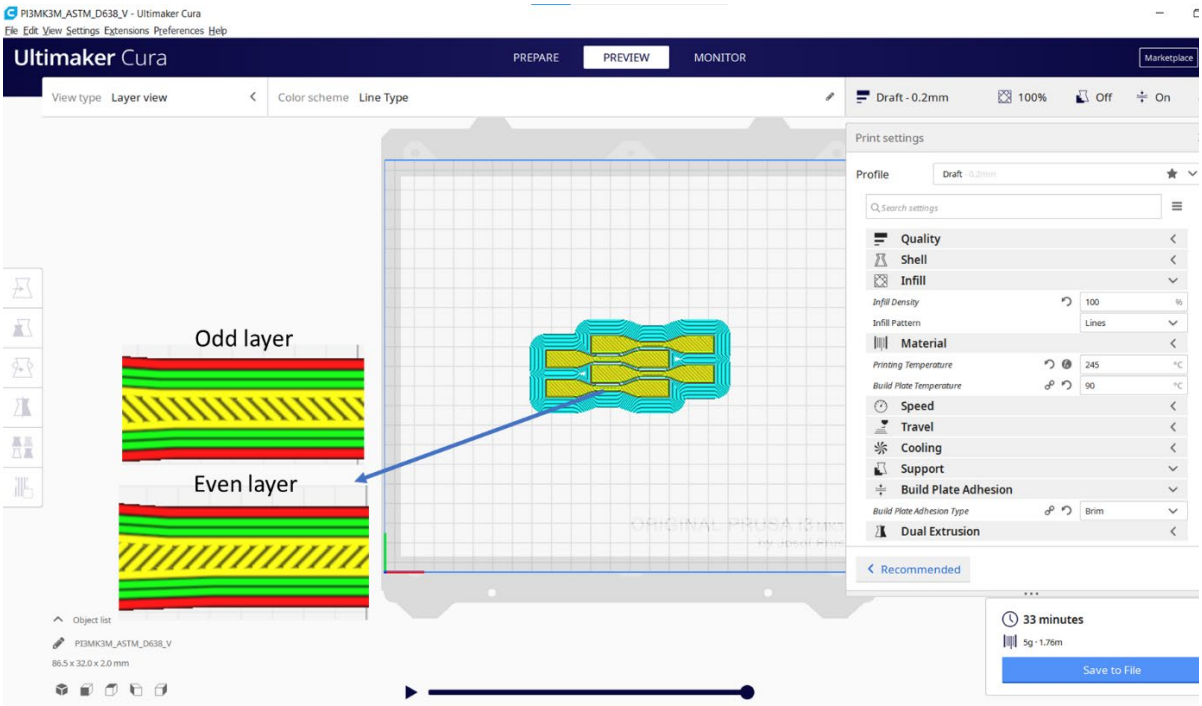

Figure 2. Slicing from Cura for Prusa with specimens manufactured in 33 minutes using 5 grams of material.

In Figure 2, the slicing process for FDM is depicted, showcasing an infill parameter configured at 100%. This deliberate choice is aimed at achieving the utmost density for the targeted layer height. Specifically, in the context of Draft mode, where layers are set at 0.2 mm thickness, the intricate composition involves the incorporation of 10 individual layers.

In Figure 3, the SLA slicing process is shown for Objet 30 Prime printer, encompassing 27 layers in total. Among these, 20 layers, each measuring 0.1 mm, constitute the part, while an additional 7 layers are dedicated to the base for secure platform attachment.

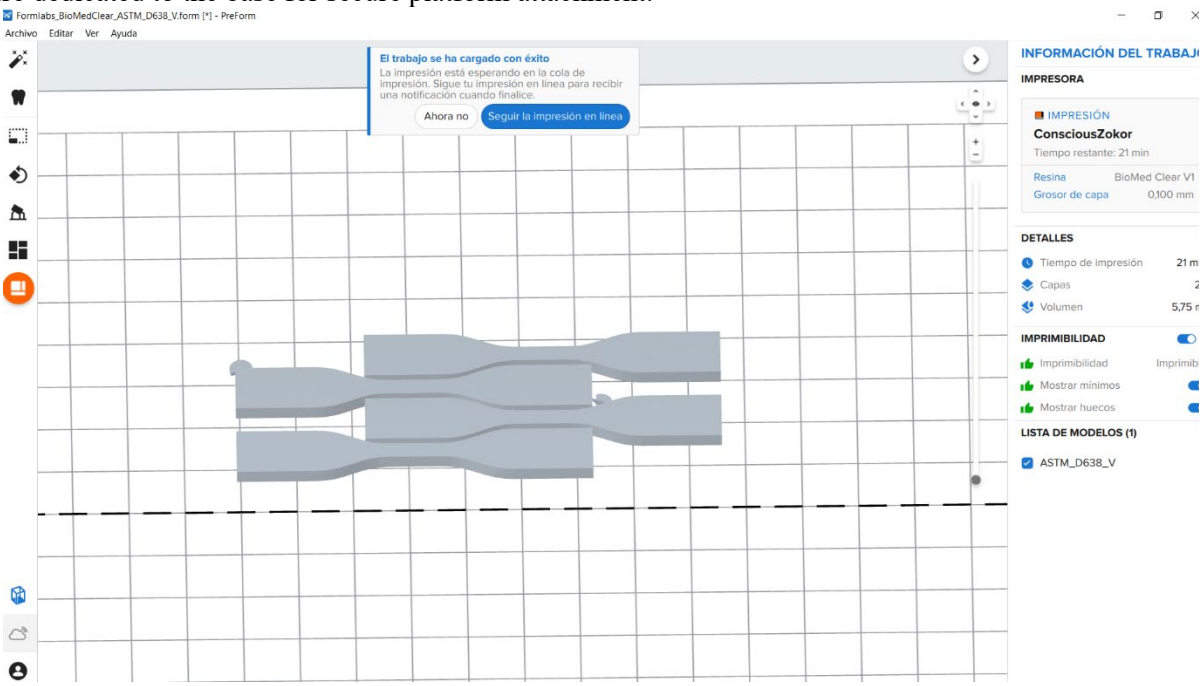

Figure 3. Slicing from Preform for Formlabs BioMed clear V1 specimens manufactured in 21 minutes using 5.75 grams of material.

2.3. Time and cost

For each individual setup involving four specimens, a multitude of adjustable parameters employs a discernible impact on manufacturing time. Delving into the realm of cost considerations, the calculations are meticulously derived from the operational experience garnered over the machine's working hours, aimed at spreading the acquisition cost across a seven-year utilization span. To illustrate, envision a machine operational for 500 hours annually. In this instance, the calculation unfolds as follows: 500 hours × 7 years = 3500 working hours. If the original machine cost tallies to €7000, this translates to a cost apportionment of €7000 / 3500h = €2/h = €0.033/min. This column is shown in table 1 and can be changed in Excel file to be downloaded from the material database.

Encompassing these numbers, the equation further incorporates the inclusion of maintenance costs and energy expenditures, yielding the comprehensive cost per minute. Other overhead costs, including labour costs, are not considered because of the substantial differences among geographical regions. It is an attempt to standardize results for comparison purposes.

The essence of the database's design lies in its adaptability, offering users the latitude to configure their cost parameters in harmony with their distinct machine utilization patterns. This dynamic feature underpins the very essence of the database, placing the power to customize cost considerations squarely in the hands of individual users.

Expanding the ambit to material costs, the calculation includes the expenditure of acquiring material while considering the tangible utilization within a tank. On the realm of FDM filament, approximately 80% of material finds purpose, while a portion is forfeited to failed tests and material replacements. Similarly, for object's material, nearly 40% is lost during washing and material replacement. These empirical experiences intricately factor into the determination of real material costs. Therefore, the true cost of each material must be calibrated to reflect these practical realities, mirroring the authenticity of the user's experience.

2.4. Tensile test

Consistency and rigor establish the testing methodology for all tensile specimens, aligning with the established protocol outlined by ASTM D638: Standard Test Method for Tensile Properties of Plastics. Employing an MTS insight equipped with a 10 kN load cell, the testing transpires at a controlled displacement rate of 10 mm/min, meticulously capturing data at a frequency of 50 Hz. This data acquisition, amounting to 300 test points over a 1 mm displacement (1/25=4%) in 60 seconds, ensures a granular understanding of the mechanical response.

Each specimen's grip displacement, load cell force, and time are meticulously documented throughout the testing process, forming a comprehensive data repository. Stress and strain calculations are rendered feasible through engineering equations that presuppose low strain and a uniform cross-section. This foundational approach allows the derivation of these crucial mechanical properties with precision, laying the groundwork for insightful analyses and robust conclusions.

To calculate stress and strain, engineering equations assuming low strain and constant section were used as follows.

$$\sigma = \frac{F}{A} \tag{1}$$

where σ is stress, F is force from tensile test machines and A is cross section area assumed to be constant during the test.

$$\epsilon = \frac{U}{L} \tag{2}$$

where ϵ is strain, U is displacement from tensile test machines and L is gauge length assumed to be constant during the test. Please note that changing in calculations L from 10 to 20 mm would imply to obtain a doubled Young's modulus. For all specimens the same L=25 mm was used even though some specimens showed early necking with deformation localised on small length. However, it was considered of interest to always compare the same force-displacement behaviour and therefore all tests used the same cross section and gage length.

3. Results

The material database serves as a repository that stores an array of material tests, facilitating comprehensive comparisons across variables such as materials, printers, and costs. Essential mechanical properties like Young's Modulus, yield stress, ultimate stress, and energy can be juxtaposed for insightful analyses. Throughout all tests conducted, the highest recorded force reached 0.8 kN (approximately 125 MPa), which remained well within the range accommodated by the 10 kN load cell. However, certain soft materials, including Formlabs Flexible 80A and Objet TangoGray, exhibited a greater degree of noise in load measurements compared to the optimal capacity of the current load cell. Despite encountering maximum loads of 0.04 kN (around 6.25 MPa) for these softer materials, the decision was made to retain the same load cell for the sake of maintaining uniformity across the comparisons.

Figure 4a, shows a snapshot of the material database, illustrating the meticulous documentation of each printer and material. Each column is a material, printer and setup providing in each row material properties from literature and measured. This documentation encompasses slicing snapshots, downloadable manufacturing files, and material datasheets from providers, fostering seamless comparisons.

The material database further facilitates the generation of diverse graphs, exemplified in Figure 4b, which plots yield stress against cost. With the added benefit of an available EXCEL file for the material database, the manipulation of material and printer costs becomes an effortless aim. This inherent flexibility empowers users to refine outcomes based on their unique considerations, thus enhancing the utility and adaptability of the material database.

(a)

		MIN	MAX	acabado		1BFB-ABS	2BFB-PLA	3BFB-PP0_	4BFB-PP0_
				poca fuerz	0	1	2	3	4
L*(mm)		25		pendiente		BFB ABS	BFB PLA	BFB PP0_25	BFB PP0_5
w(mm)		3.18			CAD				
t(mm)		2		Mat (g)	3.71	3.8	3.8	3.6	3.6
v(mm/min)		1		Sop (g)		0	0	0	0
PDF file		./ASTM_D638_V.pdf		Time (min)		16	16	19	19
STL file		./ASTM_D638_V.STL		Cost time (€/min)		0.01	0.01	0.01	0.01
				Cost mat (€/g)		0.1	0.1	0.1	0.1
				Cost sup (€/g)		0.1	0.1	0.1	0.1
	calcul	0.54 €	11.00 €	Cost (€)		0.54 €	0.54 €	0.55 €	0.55 €
not doc	datasheet	26	200000	E (MPa)		1681	3309	640	640
	datasheet	2	250	sy(MPa)		39	50	19	19
	datasheet	2	560	su(MPa)		40	53	25	25
	datasheet	5	600	ef(%)		5	6	600	600
	calcul	0.125	33.07692	ey(%)		2.320048	1.511031	2.96875	2.96875
	calcul	1.6536	12720	Fe1%(N)		106.9116	210.4524	40.704	40.704
	calcul	0.25	0.25	U1%(mm)		0.25	0.25	0.25	0.25
	calcul	15	15	t1%(s)		15	15	15	15
	calcul	12.72	1590	Fy(N)		248.04	318	120.84	120.84
	calcul	0.03125	8.269231	Uy(mm)		0.580012	0.377758	0.742188	0.742188
	calcul	1.875	496.1538	ty(s)		34.80071	22.66546	44.53125	44.53125
	calcul	12.72	3561.6	Fu(N)		254.4	337.08	159	159
	calcul	1.25	150	Uu(mm)		1.25	1.5	150	150
	calcul	75	9000	tu(s)		75	90	9000	9000
	Fabrication snapshot					./BFB_ABS	./BFB_PLA	./BFB_PP0	./BFB_PP0
	Fabrication file					./BFB_ABS	./BFB_PLA	./BFB_PP0	./BFB_PP0
	Fuente Datasheet					https://w	https://fila	https://3d	https://3d
	Resultados foto				24	./BFB_ABS	./BFB_PLA	./BFB-PP0	./BFB-PP0
	measured	1	16.84	m(gr)		3.36	4.97	3.49	3.49
	calcul	0.269542	4.539084	d(gr/mm3)		0.90566	1.339623	0.940701	0.940701
	measured	3.930818	2489.518	E(MPa)		1179.245	1965.409	589.6226	252.6954
	measured	0.786164	124.4759	E+(MPa)		58.96226	98.27044	29.48113	26.53302
	measured	0.786164	59.74843	sy(MPa)		23.58491	55.03145	23.58491	15.72327
	measured	0.117925	3.930818	sy+(MPa)		1.179245	2.751572	1.179245	3.930818
	measured	0.786164	55.03145	su(MPa)		22.01258	55.03145	26.72956	15.72327
	measured	0.117925	3.144654	su(MPa)		1.100629	2.751572	1.336478	0.786164

3DP-Materials | Control | Elastic Modulus vs € | Elastic Modulus vs density | Yield stress vs € | Yield stress vs density

(b)

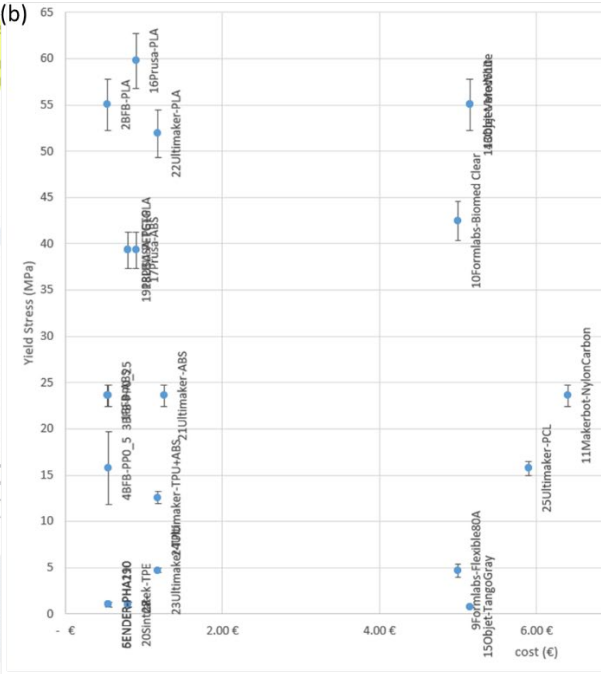

Figure 4. Example of data on material database (a) and figure for yield stress versus cost (b).

The material database is producing results in a simplified model material based on a straight elastic line of Young's modulus E up to yield stress σ_y and another straight line to ultimate stress σ_u and fracture strain ε_f. Figure 5, shows 9 different tensile tests performed on Prusa-PLA material with the same fabrication file. Finally, a PRUSA PLA-model is obtained considering E=2490±125 MPa, σ_y=59.5±3 MPa, σ_u=52.0±2.5 MPa and ε_f=4.0±0.8 %. These error bars are also shown in figure 4b.

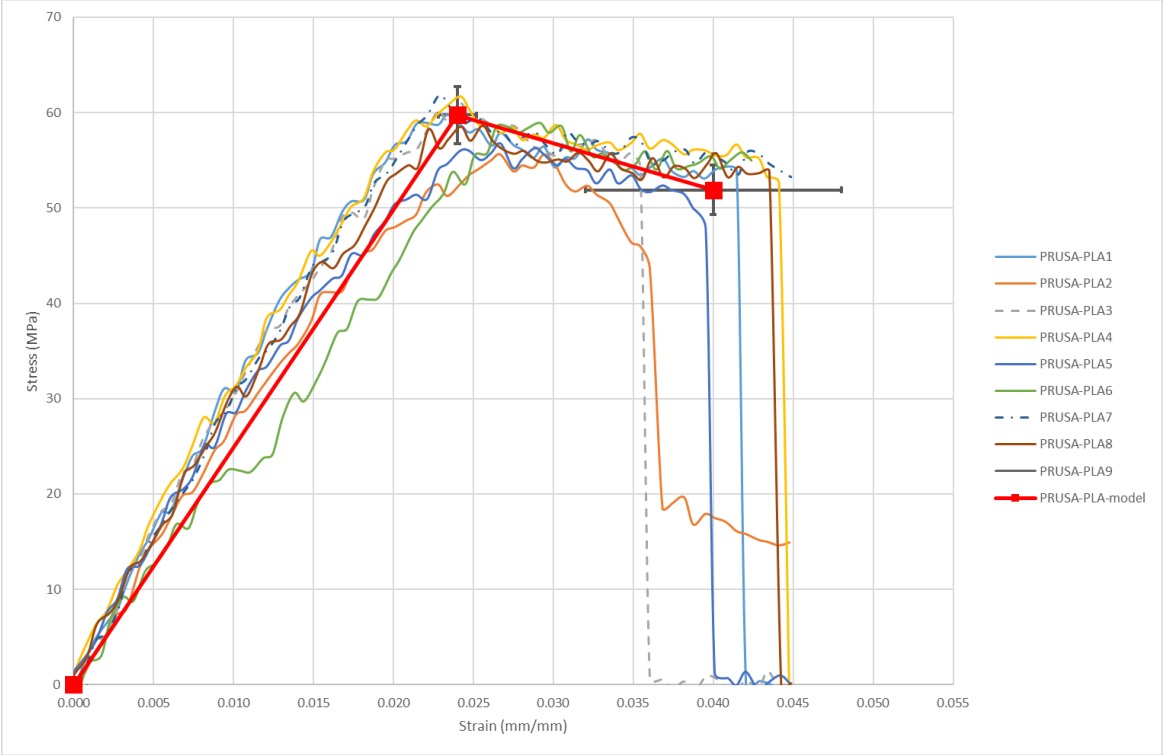

Figure 5. Stress strain curve for PRUSA PLA specimens to obtain variability.

After establishing an extensive overview of the fundamental parameters extracted from various sets of tensile curves, the subsequent step involves a comprehensive analysis of these parameters in relation to a range of relevant factors. These factors encompass density, cost, and variability, among others. Through this multi-faceted analysis, a deeper understanding emerges, shedding light on the intricate correlations and dependencies that underlie the mechanical behavior of the printed materials.

3.1. Elastic modulus

The elastic modulus, a fundamental metric, is derived by calculating the slope of the stress-strain curve. While there are distinct definitions for tangent and secant modulus within the realm of polymers, we opt for simplicity by employing a linear fit, illustrated in Figure 5, up to the yield stress.

Upon conducting this analysis across all specimens, the outcomes are synthesized into plots that offer insightful visualizations. These plots showcase the elastic modulus as a function of density in Figure 6a, and as a function of cost in Figure 6b. To elucidate the relationship between elastic modulus and density, reference lines are incorporated, demonstrating a proportional increase—when density doubles, elastic modulus also doubles.

Remarkably, within this framework, Ultimaker-PLA emerges as an exemplar, exhibiting a particularly favorable elastic modulus-to-density ratio. The same methodology is applied to cost considerations, revealing BFB-PLA's supremacy in the elastic modulus-to-cost ratio.

In essence, this systematic procedure not only determines the interplay between elastic modulus, density, and cost but also covers it within a visual narrative. These comparative insights serve as a compass, steering decisions towards materials that offer optimal trade-offs between elastic modulus, density, and cost parameters.

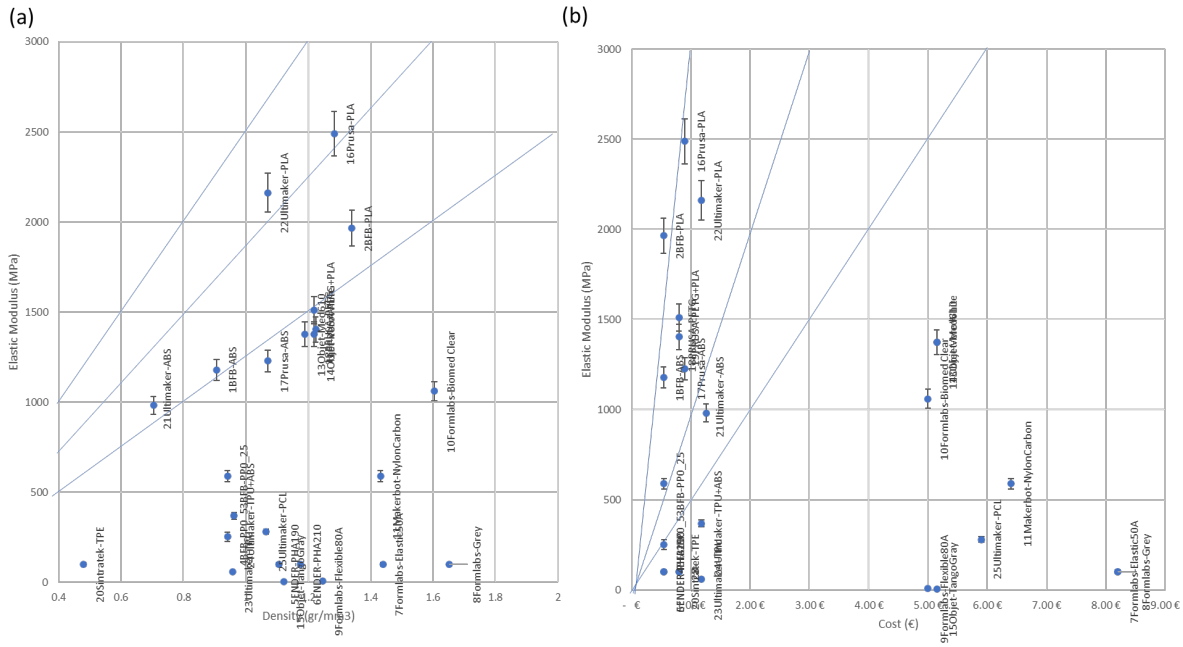

Figure 6. Elastic modulus versus density (a) and versus cost (b).

3.2. Yield stress

Yield stress is deduced through the simplification of the stress-strain curve. As depicted in Figure 7a, a discernible pattern emerges: Ultimaker-PLA boasts the most favorable yield stress-to-density ratio. Similarly, Figure 7b unveils another crucial insight: BFB-PLA emerges as the leader in the yield stress-to-cost ratio.

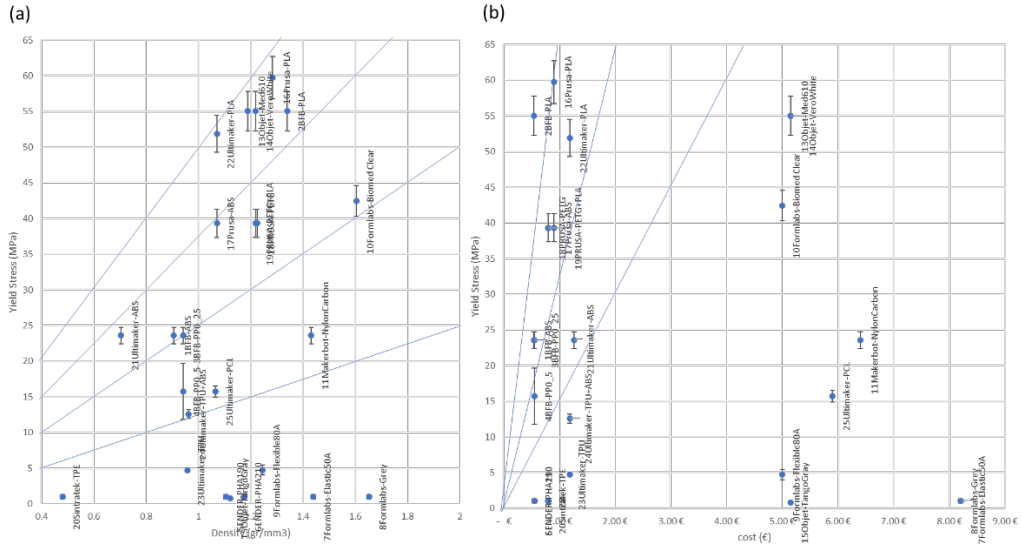

Figure 7. Yield stress versus density (a) and versus cost (b)..

3.3. Energy

Energy is computed by quantifying the area below the stress-strain curve, expressed in units of N/mm², mJ/mm³, or MJ/m³. To enable more meaningful comparisons, we normalize this energy by dividing it

by the actual density of the component, resulting in units of mJ/g or J/kg. Notably, the highest energy yield is achieved by BFB-PP, a standout performer for both 0.5 mm and 0.25 mm layer thicknesses, as depicted in Figure 8a. This elevated energy output can be attributed to the substantial deformation witnessed prior to fracture.

Interestingly, upon normalization by density, Figure 8b illustrates that there isn't a substantial shift in the observed trends. This suggests that, even when considering the influence of density, BFB-PP retains its position as the leader in energy-to-mass ratios. This stability underscores the robustness of BFB-PP's performance across varying contexts, further solidifying its position as an exceptional energy-absorbing material.

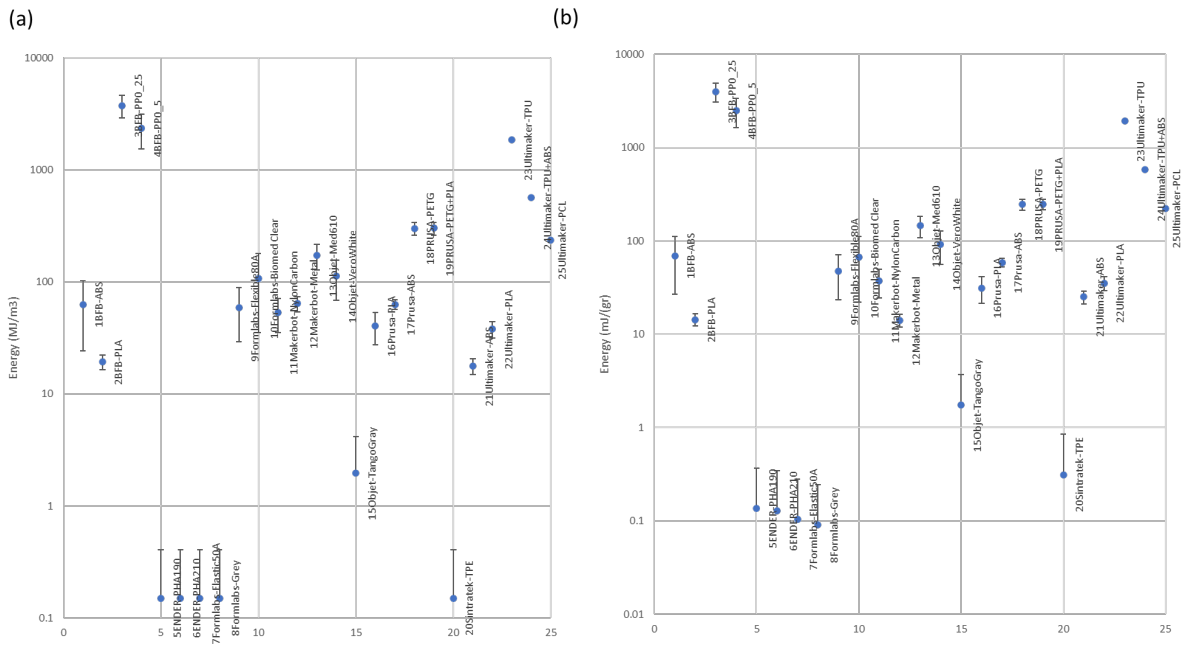

Figure 8. Energy for each material tested (a) and normalised for weight (b).

3.4. Stress strain for simplified models

Concluding our analysis, stress-strain relationships for all materials are visually represented using simplified models and a logarithmic scale, enclosed in Figure 9. The congruence with our previous findings is immediately apparent: Prusa-PLA prominently exhibits the highest Young's Modulus and yield stress, mirroring the observations in Figure 6. Similarly, the exceptional fracture strain of BFB-PP, as illustrated in Figure 8, is reaffirmed in this comprehensive depiction.

It is, however, prudent to acknowledge the unique case of Objet TangoGray and Formlabs-Elastic50A. Their values, although presented, warrant a note of caution as they should ideally be validated using a more suitable and smaller load cell. This consideration speaks to the inherent complexities that can arise when handling materials of distinct softness or flexibility and serves as a reminder of the nuanced approaches often required in their examination.

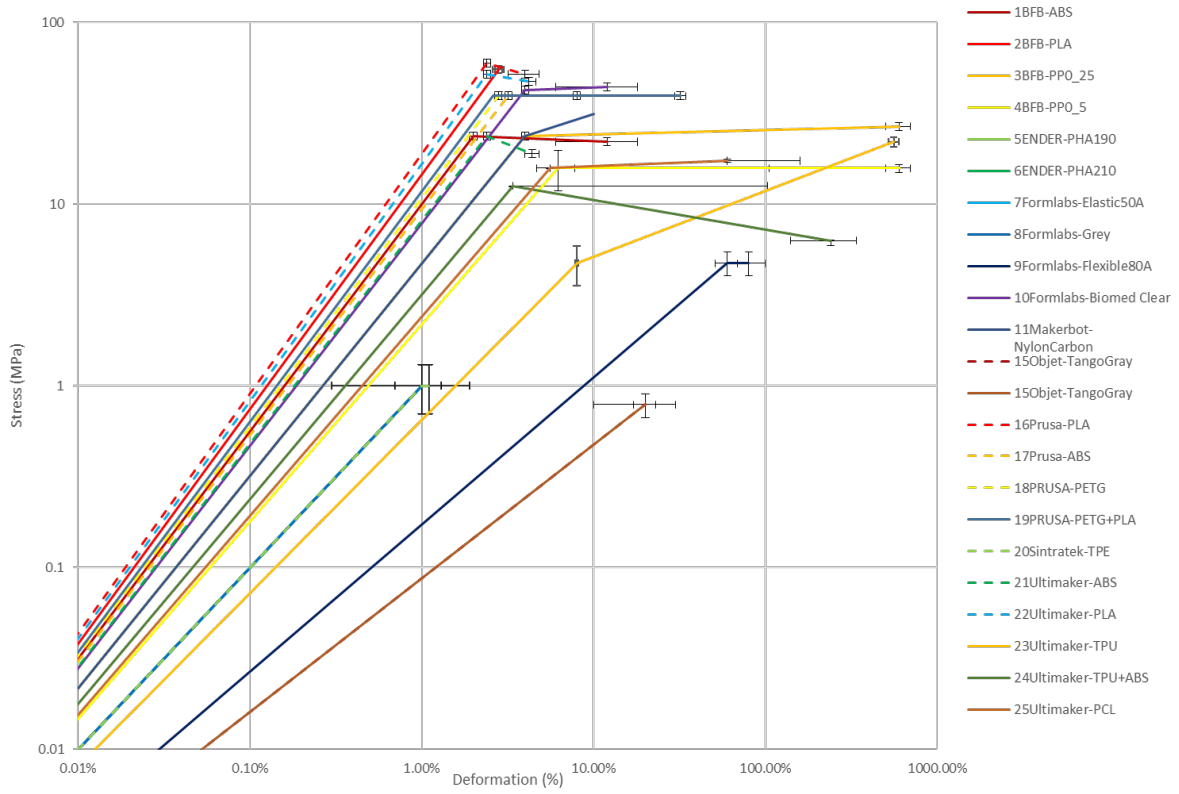

Figure 9. Stress strain for simplified models.

4. Conclusions

Concluding this study, we have constructed a comprehensive material database that establish the principle of reproducibility. In this repository, a minimum of four specimens per fabrication file have been meticulously tested and documented. The adoption of a smaller specimen design for these tensile tests has allowed for reasonable resource management in terms of material and manufacturing time. However, it's important to note that this choice does impose limitations on certain parameters, particularly regarding infill design for experiments.

The material database is thoughtfully designed to facilitate user interaction and adaptation. Available for download in Excel format, it offers the flexibility to adjust material selections and manufacturing costs, thereby aligning with individual user experiences and needs.

From our initial set of experiments, several valuable conclusions have emerged:

- The variation within Young's modulus, yield stress, and ultimate stress remains acceptable within a 10% range, but there's a noticeable 80% scatter in fracture strain, significantly impacting energy absorption.
- Among printed specimens, Ultimaker-PLA leads in the ratio of Young's modulus to density, followed by Prusa-PLA.
- In terms of the ratio of Young's modulus to IQS (industrial quality standards) cost, BFB-PLA takes the lead, trailed by Prusa-PLA.
- Yield stress to density ratio highlights Ultimaker-PLA as a frontrunner, with Objet-MED and Objet-VeroWhite trailing closely.
- The ratio of yield stress to IQS cost identifies BFB-PLA as superior, followed by PRUSA-PLA.

- BFB-PP emerges as the top contender for energy absorption, evident for both 0.5 and 0.25 mm layer thickness.
- The creation of simplified stress-strain curves, presented in logarithmic scale with error bars, provides a succinct yet comprehensive means of comparing all materials.

This database marks a foundational step towards establishing a repository for reproducible experiments, supported by consistent testing procedures. As we advance, this resource holds the potential to foster deeper insights, impulse innovation, and facilitate the development of new materials and processes within the realm of additive manufacturing.

References

[1] T.D. Ngo, A. Kashani, G. Imbalzano, K.T.Q. Nguyen, D. Hui, "Additive manufacturing (3D printing): A review of materials, methods, applications and challenges," *Composites Part B: Engineering*, vol. 143, pp. 172-196, 2018, doi:10.1016/j.compositesb.2018.02.012.

[2] M. Bhuvanesh Kumar, P. Sathiya, "Methods and materials for additive manufacturing: A critical review on advancements and challenges," *Thin-Walled Structures*, vol. 159, 2021, doi:10.1016/j.tws.2020.107228.

[3] D. Bourell, J.P. Kruth, M. Leu, G. Levy, D. Rosen, A.M. Beese, A.C., "Materials for additive manufacturing," CIRP Annals, vol. 66, pp. 659-681, 2017, doi:10.1016/j.cirp.2017.05.009.

[4] F. Calignano et al., "Overview on Additive Manufacturing Technologies," in Proceedings of the IEEE, vol. 105, no. 4, pp. 593-612, April 2017, doi: 10.1109/JPROC.2016.2625098.

[5] R. Kumar, M. Kumar and J.S. Chohan, "Material-specific properties and applications of additive manufacturing techniques: a comprehensive review". *Bull Mater Sci* 44, 181 (2021). doi:10.1007/s12034-021-02364-y.

[6] A. A. Garcia-Granada, J. Catafal-Pedragosa, and H. G. Lemu, "Topology optimization through stiffness/weight ratio analysis for a three-point bending test of additive manufactured parts," in *IOP Conference Series: Materials Science and Engineering*, 2019, vol. 700, no. 1, doi: 10.1088/1757-899X/700/1/012012.

[7] P.K. Penumakala, J. Santo, A. Thomas, "A critical review on the fused deposition modeling of thermoplastic polymer composites," *Composites Part B: Engineering*, vol. 201, 2020, doi:10.1016/j.compositesb.2020.108336.

[8] M. Domingo-Espin, J. M. Puigoriol-Forcada, A. A. Garcia-Granada, J. Llumà, S. Borros, and G. Reyes, "Mechanical property characterization and simulation of fused deposition modeling Polycarbonate parts," *Mater. Des.*, vol. 83, pp. 670–677, 2015, doi: 10.1016/j.matdes.2015.06.074.

[9] A. Sola, W.J. Chong, D.P.Simunec, Y. Li, A. Trinchi a, I. Kyratzis, C. Wen "Open challenges in tensile testing of additively manufactured polymers: A literature survey and a case study in fused filament fabrication," *Polymer Test.* vol. 117, 2023, doi:10.1016/j.polymertesting.2022.107859.

[10] D. Fico, D. Rizzo, R. Casciaro, C.C.Esposito, "A Review of Polymer-Based Materials for Fused Filament Fabrication (FFF): Focus on Sustainability and Recycled Materials". *Polymers (Basel).* 2022 Jan 24;14(3):465. doi: 10.3390/polym14030465. PMID: 35160455; PMCID: PMC8839523.

[11] B. Arifvianto, B.E. Satiti, U.A. Salim, et al. "Mechanical properties of the FFF sandwich-structured parts made of PLA/TPU multi-material". *Prog Addit Manuf* 7, 1213–1223 (2022). https://doi.org/10.1007/s40964-022-00295-6.

[12] E. Dimla, J. Rull-Trinidad, A. A. Garcia-Granada, and G. Reyes, "Thermal comparison of conventional and conformal cooling channel designs for a non-constant thickness screw cap," *J. Korean Soc. Precis. Eng.*, vol. 35, no. 1, 2018, doi: 10.7736/KSPE.2018.35.1.95.

[13] A. G. Salazar-Martín, A. A. García-Granada, G. Reyes, G. Gomez-Gras, and J. M. Puigoriol-Forcada, “Time-Dependent Mechanical Properties in Polyetherimide 3D-Printed Parts Are Dictated by Isotropic Performance Being Accurately Predicted by the Generalized Time Hardening Model,” *Polymers (Basel)*., vol. 12, no. 3, p. 678, Mar. 2020, doi: 10.3390/polym12030678.
[14] M. Criado-Gonzalez, A. Dominguez-Alfaro, N. Lopez-Larrea, N. Alegret, & D. Mecerreyes. “Additive manufacturing of conducting polymers: recent advances, challenges, and opportunities.” *ACS Applied Polymer Materials*, vol. 3, no. 6, p. 2865-2883, Jun. 2021, doi: 10.1021/acsapm.1c00252.